Alkaline Earth Metal-Organic Frameworks with Tailorable Ion Release: A Path for Supporting Biomineralization

*Maria A. Matlinska[1], Michelle Ha[1], Bryden Hughton[1], Anton O. Oliynyk[1], Abishek K. Iyer[1], Guy M. Bernard[1], Gareth Lambkin[1], Mason C. Lawrence[2], Michael J. Katz[2], Arthur Mar[1] and Vladimir K. Michaelis[1,]**

1-Department of Chemistry, University of Alberta, Edmonton, Alberta, T6G 2G2, Canada

2-Department of Chemistry, Memorial University of Newfoundland, St. John's, Newfoundland, A1C 5S7, Canada

*Corresponding author: vladimir.michaelis@ualberta.ca

Keywords: MOF, structure, porous, XRD, NMR, strontium, BSA, calcium

ABSTRACT

An innovative application of metal-organic frameworks (MOFs) is in biomedical materials. To treat bone demineralization, which is a hallmark of osteoporosis, biocompatible MOFs (bioMOFs) have been proposed in which various components, such as alkaline-earth cations and bisphosphonate molecules, can be delivered to maintain normal bone density. Multicomponent bioMOFs that release several components simultaneously at a controlled rate thus offer an attractive solution. We report two new bioMOFs, comprising strontium and calcium ions linked by p-xylylenebisphosphonate molecules, that release these three components and display no cytotoxic effects on human osteosarcoma cells. Varying the Sr^{2+}/Ca^{2+} ratio in these bioMOFs causes the rates of ions dissolving into simulated body fluid to be unique; along with the ability to absorb proteins, this property is crucial for future efforts in drug-release control and promotion of mineral formation. The one-pot synthesis of these bioMOFs demonstrates the utility of MOF design strategies.

INTRODUCTION

Osteoporosis is a debilitating disorder that affects about 200 million people worldwide, causes more than 9 million fractures a year, and imposes a large economic burden on society.[1-3] The loss of bone tissue decreases bone density and endangers the skeletal system, which performs vital functions such as moving and supporting the body, protecting organs, maintaining mineral homeostasis, producing blood cells, and regulating the endocrine system.[4, 5] In a healthy skeleton, bone is constantly remodeled: aged bone is removed (bone resorption) and replaced with new tissue (bone formation).[6] Coupling these two processes tightly ensures that bone mass, hardness, and rigidity are maintained.

Osteoporosis is strongly linked to deficiencies in alkaline-earth metal phosphates, which help form and degrade skeletal tissue.[7] For example, the primary pharmaceuticals used to suppress bone dissolution are bisphosphonates, which act as anti-resorptive agents by binding to the bone surface.[8, 9] Optimal use of bisphosphonates requires adequate calcium intake. For this reason, there is increasing interest in potential therapies combining Ca^{2+} ions and bisphosphonate-based molecules as an alternative to supplying these two substances separately.[10, 11] Strontium also has a high bone affinity and is an important element to maintain optimal bone density; it is found in strontium ranelate, a pharmaceutical compound currently used in osteoporosis therapy.[12-15] We hypothesize that biomaterials containing both calcium and strontium ions in combination with bisphosphonate ligands offer properties that could help develop next-generation pharmaceutical therapies to treat bone tissue disorders.

Attractive candidates for such biomaterials are metal-organic frameworks (MOFs), which are already useful in diverse applications, including gas storage and separation, catalysis, solid electrolytes, drug storage and delivery, imaging and sensing, and many others.[16-23] "Crystal engineering" by substitution

of the metal centers and bridging organic linkers allows a property of interest to be tailored appropriately for a desired application. Unlike the other applications, the biomedical utility of MOFs remains relatively unexplored, especially in terms of assessing their biological activity and toxicity toward tissue disorders such as osteoporosis. Recently, Shi et al. prepared two MOFs containing Ca^{2+} ions coordinated by p-xylylenebisphosphonate (PXBP) ligands, of which one, $[Ca(H_2O)_3(H_2PXBP)]$, was found to be nontoxic and to stimulate *in vitro* bone formation.[24] It would be interesting to prepare derivatives of this MOF containing a combination of alkaline-earth cations to ascertain if their degradation can be controlled to result in a diverse array of biomedical materials for ion-or drug-release, mineral formation, and protein adsorption.

Here we report the preparation of $[Sr(H_2O)_3(H_2PXBP)]$ and $[SrCa(H_2O)_3(H_2PXBP)]$ through a one-pot synthesis. Their structures were characterized by X-ray diffraction (XRD) and solid-state nuclear magnetic resonance (NMR) spectroscopy. Their biophysical effects were evaluated to test the hypothesis that multicomponent bioMOFs could offer the flexibility required to control dissolution properties involved in bone mineralization.

MATERIALS & METHODS

Synthesis: Starting materials were $CaCl_2$ (>99.9%, Sigma-Aldrich), $SrCl_2$ (>99.9%, Sigma-Aldrich), and tetraethyl p-xylylenediphosphonate (>97%, TCI).

SrPAEM ([$Sr(H_2O)_3(H_2PXBP)$]) was prepared by mixing 0.9 mmol $SrCl_2$, 0.9 mmol tetraethyl-PXBP, and 10 mL of distilled water on a magnetic stirring plate for 30 min until dissolved. The solution was subsequently placed in an autoclave and heated in a furnace at 200 °C for 3 d. Once the autoclave was cooled, the resultant material was washed with distilled water, and dried under vacuum at room temperature.

SrCaPAEM ([$SrCa(H_2O)_3(H_2PXBP)$]) was prepared by mixing 0.7 mmol $SrCl_2$, 0.234 mmol $CaCl_2$, 0.293 mmol tetraethyl-PXBP, and 10 mL of distilled water. The sample was stirred on a magnetic stirring plate until dissolution, sealed in an autoclave, and heated at 170 °C for 7 d. The autoclave was cooled to room temperature and the product was collected, soaked in ethanol, and dried under vacuum at room temperature. Despite an initial Sr:Ca ratio of 0.75:025, the final composition was determined to be 1:1 based on the NMR and XRD analysis.

CaPAEM ([$Ca(H_2O)_3(H_2PXBP)$]) was prepared in a similar way to SrPAEM from a mixture of 0.9 mmol $CaCl_2$, 0.9 mmol tetraethyl-PXBP, and 10 mL of distilled water. Unlike SrPAEM, the mixture was heated in an autoclave at 170 °C for 7 d. The resulting product was soaked and washed in ethanol and dried under vacuum at room temperature.

Ethanol soaking and washing was done in order to infiltrate the pores and remove any unwanted starting materials/byproducts from the pores. Ethanol was chosen over water (the synthesis solvent), to reduce the risk of framework collapse from capillary forces. [25]

Powder X-ray Diffraction: Powder X-ray diffraction (XRD) patterns of the finely ground samples were collected on an Inel diffractometer equipped with a curved position-sensitive detector (CPS 120) and a Cu *K*α radiation source operating at 40 kV and 20 mA. Samples were mounted onto quartz sample holders and calibrated with a Si standard. Rietveld refinements (Table S1) were performed with the TOPAS Academic software package.[26] Atomic coordinates were refined, and displacement parameters were fixed based on the previous single-crystal structure of [$Ca(H_2O)_3(H_2PXBP)$]. When refined, the occupancies of the alkaline-earth site converge to unity for the end-members CaPAEM and SrPAEM, and to 0.6(1) Sr / 0.4(1) Ca for SrCaPAEM.

Solid-State Nuclear Magnetic Resonance Spectroscopy: Solid-state ^{31}P and ^{13}C NMR data were acquired on a Bruker Avance 500 NMR spectrometer equipped with a widebore superconducting 11.75 T magnet. All data were acquired under magic-angle spinning (MAS) conditions at a spinning frequency of 12-14 kHz using a 4 mm Bruker MAS NMR probe operating in double resonance mode tuned to $^{1}H/^{31}P$ or $^{1}H/^{13}C$. MAS NMR spectra were acquired using the cross-polarization method with a 4 μs π/2 pulse ($\gamma B_1/2\pi$ = 62.5 kHz) on ^{1}H, ramped Hartman-Hahn match on ^{13}C (3 ms, contact time) and ^{31}P (1 ms, contact time), 5 s recycle delay and between 256 and 4096 co-added transients. Bloch and Hahn-echo ^{31}P NMR data were acquired with a 3.5 μs π/2 pulse ($\gamma B_1/2\pi$ = 71 kHz) on ^{31}P, 200 s recycle delay and between 128 and 512 co-added transients. All data were acquired with ^{1}H decoupling ($\gamma B_1/2\pi$ = 62.5 kHz) using the two-pulse phase-modulated (TPPM)[27] decoupling scheme. ^{13}C data were referenced to TMS (δ_{iso} = 0 ppm) by setting the high-frequency peak of adamantane to 38.56 ppm[28] and ^{31}P data were referenced by setting the isotropic peak of ammonium dihydrogen phosphate (ADP) to 0.81 ppm.

Cell Tests: A human osteosarcoma MG63 cell line was used primarily to assess the toxicity and calcification ability of selected MOFs. Cells were seeded into 96-well plates at ~70% confluency and

left to settle for 24 h, supported with a 90% DMEM/F12 (1:1), 10% FBS growth medium. Solids of SrPAEM, SrCaPAEM and CaPAEM were sterilized with 70% ethanol and vacuum-dried inside a biosafety cabinet. Saturated solutions of the three samples in the growth medium with addition of antibiotic-antimycotic and 50 µg/mL L-ascorbic acid 2-phosphate sesquimagnesium salt hydrate were prepared and incubated at 37 °C for 24 h.[29] Saturated test substances, tetraethyl PXBP and ethanol, were diluted 1:8 in the growth medium plus antibiotic-antimycotic and L-ascorbic acid phosphate. Serial dilutions (1:2) were tested to a final dilution of 1:1024. Appropriate media were exchanged every 2-3 days.

Imaging: After 28 days each well was washed with 100 µL phosphate buffered saline (137 mM NaCl, 2.7 mM KCl, 10 mM Na_2HPO_4 and 2 mM KH_2PO_4. Well contents were incubated with 100 µL of a 1:10 dilution of 36.5-38% formaldehyde solution (Sigma F8775) in ultrapure water for 15 min at room temperature. Wells were then washed with 2 × 100 µL ultrapure water. Well contents were incubated with 50 µL 2% Alizarin Red S solution (2% Alizarin Red S (Alfa Aesar 42040) in ultrapure water brought to pH 4.2 with ammonium hydroxide) for 20 min. The wells were washed with 100 µL ultrapure water and the contents were kept under 100 µL of ultrapure water for imaging. Images were obtained using an Olympus CX41 microscope and a Lumenera Infinity 1 camera.

Alizarin Red S Quantitative Assay: Dry wells (water was removed from the stained wells used for imaging and the well contents were left to dry completely) were incubated with 80 µL 10% acetic acid for 30 min at room temperature. Well contents were scraped off and transferred to microcentrifuge tubes with wide-orifice micro-pipette tips. The wells were washed with 40 µL 10% acetic acid and the wash solutions were added to the tubes. The tubes were vortexed for 10 sec, incubated at 85 °C in a thermocycler for 10 min, placed in ice-water for 5 min and centrifuged at approximately 16 000×*g* for 7 min. 30 µL 10% ammonium hydroxide was added to 75 µL of supernatant in fresh tubes. The

pH was confirmed to be approximately 4.5 using pH paper. The absorbance at 405 nm was read using a BioTek Epoch 2 plate reader.

Simulated Body Fluid: Simulated body fluid (SBF) was prepared as per Kokubo et al.[30] SrPAEM, SrCaPAEM and CaPAEM samples were placed in separate vials 70 to 140 mg and 9 mL of SBF was added to each sample. Vials were placed in a water bath at 37 ^{o}C. After four days, suspensions were suction-filtered, and the recovered solid was characterized using solid-state NMR spectroscopy.

Fetal Bovine Serum Protein Adsorption Test: A saturated solution of Bovine Serum Albumin (BSA) (BioShop) in phosphate buffered saline (PBS) was prepared (115 to 147 mg BSA in 4 mL PBS). SrPAEM, SrCaPAEM and CaPAEM samples were placed in separate vials 12 to 43 mg and 4 mL of the BSA solution was added to each sample. The vials were placed in the fridge at 3 ^{o}C for 3 days. Solids were recovered through suction filtration, using a Buchner funnel and filter paper of medium porosity and were washed with minimal amount of Milli-Q water.

Scanning Electron Microscopy: The morphology of the bioMOFs before and after protein adsorption tests was observed by scanning electron microscopy (SEM, Zeiss Sigma 300 VP-FESEM) equipped with secondary and backscattered electron detectors, an in-lens electron detector, a cathodoluminescence (CL) detector, and a Bruker energy dispersive X-ray spectroscopy (EDS) system with dual silicon drift detectors each with an area of 60 mm^2 and a resolution of 123 eV. Conductive carbon coating was applied to samples prior to image acquisition, using a Leica EM SCD005 evaporative carbon coater.

Gas Adsorption: N_2 gas adsorption isotherm data were collected at 77 K on a Micromeritics Tristar II surface area and porosity analyzer. All samples were activated on a Micromeritics Smart VacPrep instrument by initially heating the sample to 90 °C (5 °C/min) with slow evacuation (5 mm Hg/s). The sample was maintained at this temperature and low pressure for 30 mins. After this time, the

temperature was ramped to 120 °C (5 °C/min) and maintained for 10 h. The sample was then cooled to room temperature after which the sample holder was backfilled with nitrogen gas before N_2 gas adsorption analysis was carried out.

RESULTS

Three materials were prepared by hydrothermal methods in which chloride salts of Ca^{2+} or Sr^{2+} were reacted with tetraethyl-PXBP (Figure S1) in autoclaves heated at either 170 (CaPAEM, CaSrPAEM) or 200 °C (SrPAEM) for several days. The Sr-containing ([$Sr(H_2O)_3(H_2PXBP)$]; abbreviated as SrPAEM, strontium phosphonate alkaline-earth metal MOF), and the heterometallic Sr/Ca-containing ([$SrCa(H_2O)_3(H_2PXBP)$], abbreviated as SrCaPAEM) bioMOFs are new. The previously reported Ca-containing material ([$Ca(H_2O)_3(H_2PXBP)$]; abbreviated as CaPAEM) was resynthesized to serve as a reference.

STRUCTURE

The new materials SrPAEM and SrCaPAEM were characterized by a combination of powder XRD and NMR spectroscopy to determine both the long- and short-range structure (Figure 1). The similarity of the powder XRD patterns (Figure 1a) indicates that these compounds are isostructural to the previously reported Ca-containing material CaPAEM. Rietveld refinements (Table S1) confirm a monoclinic structure (in space group *C*2/*c*) in which protonated PBXP (one proton per phosphate) ligands and water molecules surround the alkaline-earth cations to form a seven-coordinate metal cation (Figure 2). On progressing from CaPAEM to SrPAEM, the unit cell volume increases by 9% and each of the cell lengths increases by about 3%, consistent with the relative sizes of the alkaline-earth cations (Shannon ionic radii of 1.06 Å for Ca^{2+} and 1.21 Å for Sr^{2+} in CN7).[31] The peaks for SrCaPAEM are slightly wider than those for SrPAEM and CaPAEM, which might suggest some

inhomogeneity of the solid solution. Other factors such as crystallite size in nanomaterials can also broaden lines, but these crystals are on the micron scale.

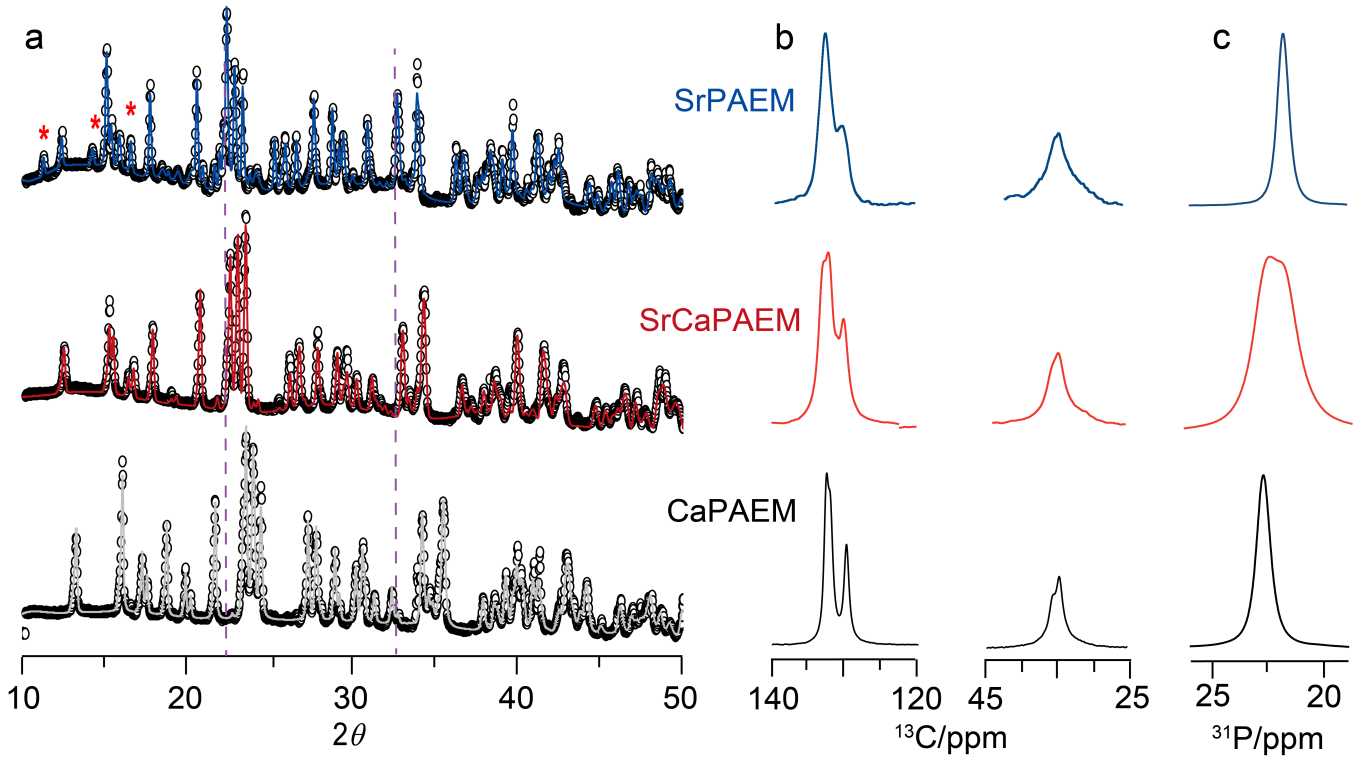

Figure 1. (a) Powder XRD patterns (observed: circles; fits: lines; asterisks: secondary phases, purple dashed lines are guides for the eye), (b) ^{13}C and (c) ^{31}P cross polarization magic-angle spinning NMR spectra for SrPAEM (blue), SrCaPAEM (red), and CaPAEM (black).

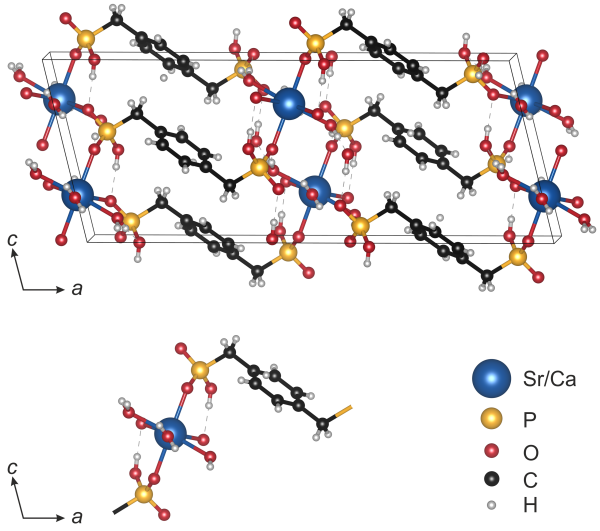

Figure 2. Crystal structure and asymmetric unit of SrPAEM, SrCaPAEM and CaPAEM.

For the heterometallic bioMOF SrCaPAEM, the XRD pattern clearly shows Bragg diffraction located at 2θ angles intermediate between those of the end-members CaPAEM and SrPAEM, implying that the sample contains a single phase with a statistical mixture of Ca^{2+} and Sr^{2+} ions occupying the unique alkaline-earth metal site (Figure 1 and Figure S2). The refined cell parameters are intermediate; if Vegard's law is assumed, a linear interpolation suggests that the composition is slightly Sr-richer, corresponding to $x = 0.3$ in the formula $[Sr_{1-x}Ca_x(H_2O)_3(H_2PXBP)]$. If the occupancy of the alkaline-earth metal site is refined from the powder XRD data, it converges to 0.6 Sr (and 0.4 Ca), in good agreement with the conclusion from the trend in cell parameters.

Solid-state NMR spectroscopy is a valuable method to further probe the local atomic structure of these materials, complementing the long-range structural insight from diffraction studies. Analysis of the NMR spectra reveals how the bisphosphonate ligands are affected in the series of materials SrPAEM, SrCaPAEM, and CaPAEM. The ^{13}C cross-polarization magic-angle spinning (CP MAS) NMR spectra confirm that the ethyl functional groups (observed at 16 and 62 ppm; Figure S3) in the tetraethyl-PXBP ligands are hydrolyzed (i.e., no resonances are observed for the ethyl groups) during the hydrothermal synthesis of these compounds.[32] In looking at the CaPAEM, SrPAEM, and SrCaPAEM, the isotropic

chemical shifts (δ_{iso}) for the ortho-methylene bridging C atoms appear at ~35 ppm, and those for the three unique aromatic C atoms are located between 130 and 135 ppm (Figure 1b and Figure S3). Substitution of Ca for Sr impacts the aromatic ^{13}C resonances, where the methine (-CH=; $\delta_{iso}(^{13}C)$~135 ppm) carbon shifts to lower frequency, while the lowest frequency aromatic ^{13}C resonance ($\delta_{iso}(^{13}C)$~130 ppm) shifts to higher frequency decreasing the resolution between the C2, C3, and C4 resonances (Figure 1b). To further understand the change in the aromatic region, gauge including projector augmented waves (GIPAW) density functional theory (DFT) calculations were performed.[33-35] The crystal structures were geometry optimized, and then the NMR interactions (^{13}C shielding) were calculated (Table S2). For SrPAEM, the highest frequency resonance is shielded by ~2 ppm while the lowest frequency resonance exhibits a deshielding effect when compared to CaPAEM, in agreement with the interpretation of the experimental NMR spectra. As expected, the ^{13}C MAS NMR spectrum of SrCaPAEM exhibits isotropic chemical shifts part way between the two parent compounds.

The ^{31}P CP MAS NMR spectra show sharp and distinct single resonances with δ_{iso} = 22.8 ppm for CaPAEM and 21.8 ppm for SrPAEM (Figure 1c), consistent with the presence of a unique P site in the crystal structure. The shift to lower frequency in SrPAEM vs. CaPAEM is supported by GIPAW DFT calculations ($\Delta\delta_{iso}(^{31}P)_{calc.}$ = 1.5 ppm, Table S2). For the heterometallic compound SrCaPAEM, the resonance is located nearly in the middle ($\delta_{iso}(^{31}P)$ = 22.3 ppm) between those for the end-members CaPAEM and SrPAEM, implying that the MOF consists of a single phase containing a statistical mixture of Ca^{2+} and Sr^{2+} ions in the alkaline-earth metal site, as opposed to a mixture of the two end-members. Moreover, the full-width-at-half-maximum (FWHM) of the resonance for SrCaPAEM is larger and not reproducible from a physical mixture or sum of the spectra for the end-members, vide infra. This broadening of the isotropic resonance clearly suggests disorder of the environment around the P atoms, to which the Ca^{2+} and Sr^{2+} ions are in proximity. When a two-site Gaussian deconvolution

of this resonance is applied and the linewidth and chemical shift are adjusted, a composition of 0.48 Sr / 0.52 Ca is obtained (with a 10% error). This conclusion agrees with the XRD results, where a composition of 0.6 Sr / 0.4 Ca (with a 12% error) is obtained. It is interesting that this composition deviates from the nominal composition (0.75 Sr / 0.25 Ca) used in the hydrothermal synthesis, suggesting that kinetic factors may be at play to favor the incorporation of the smaller Ca^{2+} ion.

BIOPHYSICAL PROPERTIES

Effects on human osteosarcoma cells

Many bone tissue disorders are linked to the depletion of calcium; successful markers for biomaterials may include an ability for ion-release, calcification, non-toxicity, and affinity to adsorb proteins. Cell calcification tests were conducted using an MG63 human osteocarcoma line on CaPAEM, SrPAEM, and SrCaPAEM as bioMOF candidates and on the starting material in triplicate. Alizarin Red S may be used to identify calcium or strontium mineral deposits, indicating successful calcification. Deposits were observed in select samples (SrCaPAEM, and CaPAEM) in the initial analysis. Upon repeating Alizarin Red S tests, only the CaPAEM demonstrated staining (i.e., calcification, Figure S4) consistent with previous findings.[24] No staining was observed in the third round of testing for any of the compounds. The cause for these different observations could be related to the alkaline earth phosphate solubility; where a minimum concentration or specific range of bioMOF (i.e., Ca/Sr/P concentration) is needed to nucleate and induce crystallization. In all cases control samples (growth medium, starting material tetraethyl PXBP, ethanol, no cell) show no staining, confirming these species do not lead to calcification.

In contrast to the bioMOFs, which were completely non-toxic, the commercial tetraethyl PXBP ligand (prior to hydrolyzation) is highly toxic and killed all cells at dilutions as low as 1:128; the next two dilutions (1:256 and 1:512) resulted in cells becoming very sick. This observation, along with a

comparison of the ^{13}C and ^{31}P CP MAS NMR spectra of the tetraethyl PXBP ligand with those of the product MOFs, confirms that no excess non-hydrolyzed ligand was present in the products and all reagents reacted to completion or were washed away appropriately post synthesis. Although previous studies have indicated that the toxicity of raw materials was the key factor influencing the cytotoxicity of resulting MOFs,[36, 37] the formation of SrPAEM and SrCaPAEM runs counter to this claim, whereby the hydrolyzed ligand does not appear to influence the cells. As the resulting MOF displays no cytotoxicity, they are biologically safe even during quick dissolution of SrPAEM. Non-toxicity of bioMOFs *in vitro* is a crucial property in assessing their viability as biomaterial candidates to target bone dissolution associated with osteoporosis.

Ion release into simulated body fluid

Biosafe and biofunctional materials should also allow some degree of control over the delivery process. For an artificial material to bind to bone when implanted in a living body, an important requirement is either the formation of bone-like apatite on its surface or an ability to supply the essential minerals that can readily be used to promote apatite formation.[30] Conditions closely similar to those in a living system can be mimicked *ex situ* in a simulated body fluid (SBF), which is a solution having ion concentrations nearly equal to those of human blood plasma.[38] Simulated body fluid tests were performed on SrPAEM, SrCaPAEM, and CaPAEM by soaking them in the SBF solution and recovering solids four days later for ^{31}P CP MAS NMR analyses.

While SrPAEM dissolved completely in SBF, CaPAEM was only partially dissolved and could be recovered. The difference in solubility of these two materials arises from the composition of SBF, which contains Ca^{2+} ions at a 2.5 mM concentration, but no Sr^{2+} ions.[30] SrPAEM readily dissolves in solution to create an equilibrium concentration of Sr^{2+} ions;[39] in contrast, introducing CaPAEM into the solution, which already contains Ca^{2+} ions, causes an equilibrium shift toward solid CaPAEM by

virtue of the common-ion effect, suppressing its dissolution in SBF. These dissolution characteristics are attractive for ion-releasing therapies because Ca^{2+} and Sr^{2+} ions are readily adsorbed within the body to help form and retain bone density. We note that these ions could possibly exchange with those present in SBF (e.g., H^+, Na^+, K^+, Mg^{2+}, and Ca^{2+}). Given its smaller charge-to-size ratio, Sr^{2+} ions are expected to be less tightly bound and more likely to dissolve preferentially. The remaining MOF would shrink causing the diffraction pattern to shift towards a smaller unit cell governed by the skeletal CaPAEM structure losing crystallinity post-SBF. As such, we cannot provide evidence that alkali or alkaline earth ions from the SBF matrix are replacing the Sr positions or if charge-compensating protons are responsible. Recall that the ion release rate depends on the environment (e.g., pH, temperature, ion concentration, and ion composition) in which the material is introduced; regardless of whether the Ca^{2+} or Sr^{2+} ions are exchanged quickly or slowly, all of the solid material will eventually dissolve completely. Therefore, we propose that H^+ replaces Ca^{2+}/Sr^{2+} ions to maintain charge-compensation on the phosphate anions (i.e., acidification of the linker) as the MOF dissolves.

Qualitatively, CaPAEM dissolves slowly (solid materials are still present after >7 days), SrPAEM dissolves quickly (solid material is absent after <2 days), and SrCaPAEM dissolves at an intermediate rate. As these materials diffract poorly after SBF treatment (Figure S5), ^{31}P MAS NMR spectroscopy was used to provide atomic-level insight into the ion release and potential biomineralization process. The ^{31}P NMR spectrum of SrCaPAEM reveals isotropic chemical shifts consistent with the pre-SBF-exposed SrCaPAEM, indicating that Sr^{2+} and Ca^{2+} ions are still present after 4 days (Figure 3).

An important consideration is whether the ^{31}P NMR spectrum of SrCaPEAM is that of a solid solution or that of a mixture of SrPEAM and CaPEAM. Figure 3 (left) illustrates an expansion of the isotropic region of the ^{31}P NMR spectra for the three samples, prior to SBF treatment. The upper trace illustrates a simulation of the spectrum expected for a 1:1 mixture of SrPEAM and CaPEAM, based on the

individual spectra for these compounds. Clearly the resolution for this simulation is much greater than what is actually observed for SrCaPEAM. Likewise, post treatment, the ^{31}P NMR spectrum for this sample still consists of Ca and Sr sites, albeit with a reduced relative intensity for the lower frequency peak. But there was no detectable ^{31}P NMR signal for SrPEAM when subjected to the same treatment while that for CaPEAM was easily detected (Figure 3, right); thus the ^{31}P NMR spectrum of a mixture of these two samples would yield only a single peak at the resonance of CaPEAM, in contrast to our observations. The NMR data are consistent with the changes observed in the powder XRD data where the volume of the unit cell is between those for SrPAEM and CaPAEM, as expected for a mixed heteroatom solid solution (Figures 1 and S2). The ^{31}P NMR spectrum of SrCaPAEM post-SBF exposure shows a change in the relative intensities of the two ^{31}P peaks at ~22 and ~23 ppm after SBF testing (4 days) (Figure 3). We propose that the decrease in intensity for the peak at ~22 ppm is due to partial preferential dissolution of Sr^{2+} ions into SBF. This observation reinforces the assertion that the sample is a single phase with a mixed-metal site, vide supra.

CaPAEM shows a weak (<2%) ^{31}P resonance at δ_{iso} ~ 1.5 ppm (Figure 3, inset), which appears in the ^{31}P chemical shift range for calcium phosphate minerals such as octacalcium phosphate, dicalcium phosphate, and hydroxyapaptite.[40, 41] The ^{31}P chemical shift of 1.5 ppm suggests the formation of dicalcium phosphate dihydrate (Brushite, $CaHPO_4 \bullet 2H_2O$), based on a previous ^{31}P solid-state NMR study by Cheetham et al. where a pure mineral form has an isotropic chemical shift of 1.6 ppm.[42] This is consistent with past results on CaPAEM[24] whereby the SBF dissolution experiments demonstrated an increase in calcium concentration, eventually leading to various calcification deposits which were tentatively assigned as octacalcium phosphate and hydroxyapatite.

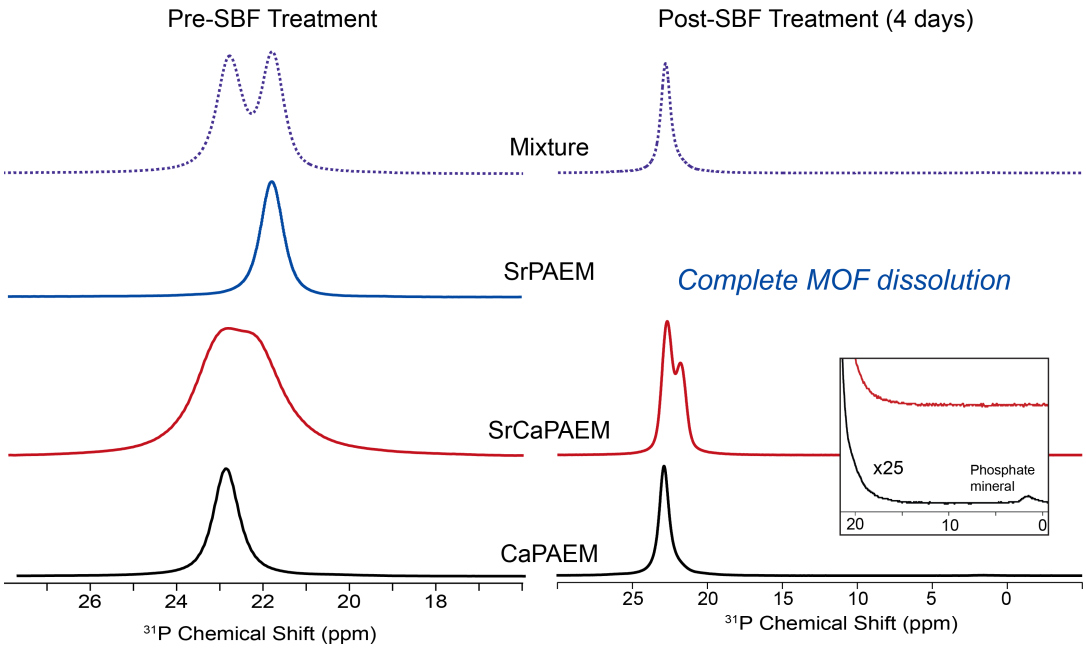

Figure 3. Phosphorus-31 CP MAS NMR spectra of CaPAEM (black); SrCaPAEM (red); and SrPAEM (blue); the purple-dashed trace is a simulation of the spectrum expected for a physical 50:50 mixture of CaPAEM and SrPAEM. MOFS pre- (left) and post- (right) SBF treatment for four days. Inset shows CaPAEM and SrCaPAEM post-SBF treatment (four days) with a vertical scale increase by 25-fold, revealing phosphate mineral formation for CaPAEM.

Porosity assessment

The porosities of the three bioMOFs were measured by nitrogen adsorption at 77 K, with data fitted according to the Brunauer-Emmett-Teller (BET) theory of gas adsorption (Figure S6). The surface areas were found to be 30 m^2/g for SrPAEM, 150 m^2/g for SrCaPAEM and 10 m^2/g for CaPAEM. Although these material do not exhibit any notable porosity, consistent with the dense crystal structure, the marked increase in the BET surface area for SrCaPAEM may be explained by the presence of small Ca^{2+} ions that now occupy larger than normal apertures in the MOF framework imposed by the

presence of larger Sr^{2+} ions, or higher degree of defects within the heterometallic compound, enabling N_2 molecules to enter the channels more readily.

Protein adsorption ability

The bioavailability potential of materials can be assessed in various ways, including research-grade blood plasma tests or via cell cultures.[43] Although a widely accepted paradigm is that SBF tests can determine bioavailability, it is important not to rely exclusively on this method. As an additional test, affinity to bovine serum albumin (BSA) was used to determine the protein adsorption of the bioMOFs *in vitro*.[44-46]

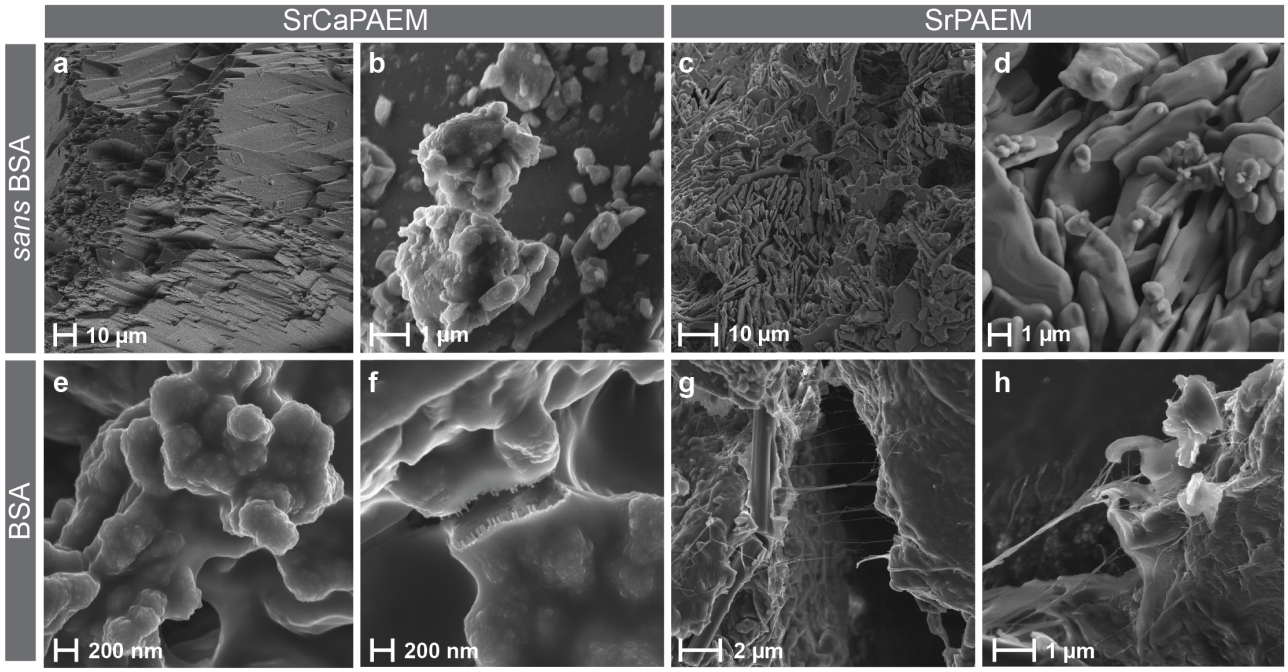

Figure 4. SEM images of SrCaPAEM and SrPAEM pre- (a-d) and post- (e-h) BSA treatment

The scanning electron microscopy (SEM) images of the materials prior to BSA treatment display rough and smooth edges as shown in Figures 4a-d. The morphology of the MOFs change drastically upon BSA treatment (Figures 4e-h) revealing smoother edges, bridging features and fiber-like structures on the surface caused by their ability to adsorb and bind bovine serum albumin protein. The BSA coating

changes the morphology of the materials and accentuates the finer crystalline elements (i.e., the teeth-looking elements in Figure 4f). This property, along with the bioavailability indicated by the SBF testing and the biosafety confirmed in cell line tests, makes the synthesized materials a promising candidate for a biological application.

CONCLUSIONS

The preparation and characterization of the isostructural Sr- and heterometallic Sr/Ca-containing derivatives of $[Ca(H_2O)_3(H_2PXBP)]$ imply the potential for other compositions $[Sr_{1-x}Ca_x(H_2O)_3(H_2PXBP)]$ may be possible. This series is biologically safe in human osteosarcoma cells with an ability to incorporate Ca^{2+} and Sr^{2+} ions, indicating their potential to combat bone demineralization and readily binds with BSA. The Sr/Ca heterometallic material partially releases Sr^{2+} ions into SBF and absorbs proteins while the CaPAEM and SrPAEM parents exchange slower and faster, respectively, suggesting that the rate of ion release may be controlled. Incorporating alkaline-earth cations and bisphosphonate molecules into a single compound allows the simultaneous supply of critical elements (Ca, Sr, P) to promote regeneration of bone tissue. This work opens new possibilities in creating a safe and biofunctional platform for targeted delivery to combat osteoporosis.

SUPPORTING INFORMATION

The Supporting Information is available free of charge on the ACS Publications website at DOI:

- Crystallographic refinements, DFT calculations, powder XRD, ^{13}C NMR, Alizarin Red S staining and BET analysis.

AUTHOR CONTRIBUTIONS

Material synthesis and experimental design: MAM, BH, VKM; Powder X-ray diffraction: MAM, AKI, AOO; NMR characterization: GMB, MAM, MH, BH; BET analysis: MCL, MJK; Simulated body fluid and protein adsorption tests: MAM; Cell tests: GL, MAM. Wrote manuscript: MAM, GMB, MJK, AM, VKM.

COMPETING INTERESTS

The authors declare no competing interests.

ACKNOWLEDGMENTS

The Natural Sciences and Engineering Research Council (NSERC) of Canada DG, RTI, and CREATE (ATUMS) programs, Canada Foundation for Innovation, and the University of Alberta are acknowledged for research support (MK, AM, and VKM). MAM was partially supported by the Dr. R. Norman and Magda Kemeny Jones Studentship. MH acknowledges NSERC for a Postgraduate Doctoral Scholarship, Alberta Innovates Graduate Scholarship and the Government of Alberta Queen Elizabeth II Scholarship. BH was partially supported by an NSERC-USRA Scholarship. The authors thank Dr. Nathan Gerein for his assistance in acquiring SEM images and Ms. Kara Meningir for her assistance in reproducing the materials to be used in BSA testing. Access to CASTEP software was provided by Dr. V. Terskikh at the National Ultrahigh-Field NMR Facility for Solids (Ottawa, Canada).

REFERENCES:

1. Johnell, O.; Kanis, J. A., An Estimate of the Worldwide Prevalence and Disability Associated with Osteoporotic Fractures. *Osteoporosis International* **2006,** *17* (12), 1726-1733.
2. Kanis, J. A. *Who Technical Report*; University of Sheffield: UK, 2007.
3. Melton III, L. J.; Chrischilles, E. A.; Cooper, C.; Lane, A. W.; Riggs, B. L., Perspective How Many Women Have Osteoporosis? *Journal of Bone and Mineral Research* **1992,** *7* (9), 1005-1010.
4. Clarke, B., Normal Bone Anatomy and Physiology. *Clinical Journal of the American Society of Nephrology* **2008,** *3* (Supplement 3), S131-S139.
5. Downey, P. A.; Siegel, M. I., Bone Biology and the Clinical Implications for Osteoporosis. *Physical Therapy* **2006,** *86* (1), 77-91.
6. Feng, X.; McDonald, J. M., Disorders of Bone Remodeling. *Annual Review of Pathology: Mechanisms of Disease* **2011,** *6* (1), 121-145.
7. Aaseth, J.; Boivin, G.; Andersen, O., Osteoporosis and Trace Elements – An Overview. *Journal of Trace Elements in Medicine and Biology* **2012,** *26* (2), 149-152.
8. Rosen, C. J.; Kessenich, C. R., Comparative Clinical Pharmacology and Therapeutic Use of Bisphosphonates in Metabolic Bone Diseases. *Drugs* **1996,** *51* (4), 537-551.
9. Drake, M. T.; Clarke, B. L.; Khosla, S., Bisphosphonates: Mechanism of Action and Role in Clinical Practice. *Mayo Clinic Proceedings* **2008,** *83* (9), 1032-1045.
10. Kennel, K. A.; Drake, M. T., Adverse Effects of Bisphosphonates: Implications for Osteoporosis Management. *Mayo Clinic Proceddings* **2009,** *84* (7), 632-638.
11. Pors Nielsen, S., The Biological Role of Strontium. *Bone* **2004,** *35* (3), 583-588.
12. Castiglioni, S.; Cazzaniga, A.; Albisetti, W.; Maier, J. A. M., Magnesium and Osteoporosis: Current State of Knowledge and Future Research Directions. *Nutrients* **2013,** *5* (8), 3022-3033.
13. Cortet, B., Strontium Ranelate: New Perspectives for the Management of Osteoporosis. *Rheumatology* **2009,** *48* (suppl_4), iv1-iv2.
14. Querido, W.; Rossi, A. L.; Farina, M., The Effects of Strontium on Bone Mineral: A Review on Current Knowledge and Microanalytical Approaches. *Micron* **2016,** *80*, 122-134.
15. Rachner, T. D.; Khosla, S.; Hofbauer, L. C., Osteoporosis: Now and the Future. *The Lancet* **2011,** *377* (9773), 1276-1287.

16. Campbell, M. G.; Dincă, M., Metal–Organic Frameworks as Active Materials in Electronic Sensor Devices. *Sensors* **2017,** *17* (5), 1108.
17. Chen, S.; Lucier, B. E. G.; Luo, W.; Xie, X.; Feng, K.; Chan, H.; Terskikh, V. V.; Sun, X.; Sham, T.-K.; Workentin, M. S.*, et al.*, Loading across the Periodic Table: Introducing 14 Different Metal Ions to Enhance Metal–Organic Framework Performance. *ACS Applied Materials & Interfaces* **2018,** *10* (36), 30296-30305.
18. Eddaoudi, M.; Kim, J.; Rosi, N.; Vodak, D.; Wachter, J.; O'Keeffe, M.; Yaghi, O. M., Systematic Design of Pore Size and Functionality in Isoreticular MOFs and Their Application in Methane Storage. *Science* **2002,** *295* (5554), 469-472.
19. Furlong, B. J.; Katz, M. J., Bistable Dithienylethene-Based Metal–Organic Framework Illustrating Optically Induced Changes in Chemical Separations. *Journal of the American Chemical Society* **2017,** *139* (38), 13280-13283.
20. Furukawa, H.; Cordova, K. E.; O'Keeffe, M.; Yaghi, O. M., The Chemistry and Applications of Metal-Organic Frameworks. *Science* **2013,** *341* (6149), 1230444.
21. Keskin, S.; Kızılel, S., Biomedical Applications of Metal Organic Frameworks. *Industrial & Engineering Chemistry Research* **2011,** *50* (4), 1799-1812.
22. Nguyen, H. G. T.; Schweitzer, N. M.; Chang, C.-Y.; Drake, T. L.; So, M. C.; Stair, P. C.; Farha, O. K.; Hupp, J. T.; Nguyen, S. T., Vanadium-Node-Functionalized UiO-66: A Thermally Stable MOF-Supported Catalyst for the Gas-Phase Oxidative Dehydrogenation of Cyclohexene. *ACS Catalysis* **2014,** *4* (8), 2496-2500.
23. Zhou, H.-C.; Long, J. R.; Yaghi, O. M., Introduction to Metal–Organic Frameworks. *Chemical Reviews* **2012,** *112* (2), 673-674.
24. Shi, F.-N.; Almeida, J. C.; Helguero, L. A.; Fernandes, M. H. V.; Knowles, J. C.; Rocha, J., Calcium Phosphonate Frameworks for Treating Bone Tissue Disorders. *Inorganic Chemistry* **2015,** *54* (20), 9929-9935.
25. Howarth, A. J.; Peters, A. W.; Vermeulen, N. A.; Wang, T. C.; Hupp, J. T.; Farha, O. K., Best Practices for the Synthesis, Activation, and Characterization of Metal–Organic Frameworks. *Chemistry of Materials* **2017,** *29* (1), 26-39.
26. BrukerAXS *Topas V4: General Profile and Structure Analysis Sofware for Powder Diffraction Data*, Bruker AXS: Karlsruhe, Germany, 2008.
27. Bennett, A. E.; Rienstra, C. M.; Auger, M.; Lakshmi, K. V.; Griffin, R. G., Heteronuclear Decoupling in Rotating Solids. *The Journal of Chemical Physics* **1995,** *103* (16), 6951-6958.

28. Earl, W. L.; Vanderhart, D. L., Measurement of ^{13}C Chemical Shifts in Solids. *Journal of Magnetic Resonance (1969)* **1982,** *48* (1), 35-54.
29. Czekanska, E. M.; Stoddart, M. J.; Richards, R. G.; Hayes, J. S., In Search of an Osteoblast Cell Model for in Vitro Research. *European Cells and Materials* **2012,** *24*, 1-17.
30. Kokubo, T.; Takadama, H., Simulated Body Fluid (Sbf) as a Standard Tool to Test the Bioactivity of Implants. In *Handbook of Biomineralization*, Bauerlein, E., Ed. 2008; pp 97-109.
31. Shannon, R. D., Revised Effective Ionic Radii and Systematic Studies of Interatomic Distances in Halides and Chalcogenides. *Acta Crystallographica Section A* **1976,** *32* (5), 751-767.
32. Ernst, L., ^{13}C N.M.R. Spectroscopy of Diethyl Alkyl- and Benzyl-Phosphonates. A Study of Phosphorus–Carbon Spin–Spin Coupling Constants over One to Seven Bonds. *Organic Magnetic Resonance* **1977,** *9* (1), 35-43.
33. Clark, S.; Segall, M.; Pickard, C.; Hasnip, P. J.; Probert, M. I. J.; Refson, K.; Payne, M. C., First Principles Methods Using Castep. *Zeitschrift für Kristallographie - Crystalline Materials* **2009,** *220* (5/6), 567-570.
34. Pickard, C. J.; Mauri, F., All-Electron Magnetic Response with Pseudopotentials: NMR Chemical Shifts. *Physical Review B* **2001,** *63* (24), 245101.
35. Yates, J. R.; Pickard, C. J.; Mauri, F., Calculation of NMR Chemical Shifts for Extended Systems Using Ultrasoft Pseudopotentials. *Physical Review B* **2007,** *76* (2), 024401.
36. Horcajada, P.; Chalati, T.; Serre, C.; Gillet, B.; Sebrie, C.; Baati, T.; Eubank, J. F.; Heurtaux, D.; Clayette, P.; Kreuz, C.*, et al.*, Porous Metal–Organic-Framework Nanoscale Carriers as a Potential Platform for Drug Delivery and Imaging. *Nature Materials* **2009,** *9*, 172.
37. Liu, R.; Yu, T.; Shi, Z.; Wang, Z., The Preparation of Metal-Organix Frameworks and Their Biomedical Application. *International Journal of Nanomedicine* **2016,** *11*, 1187-1200.
38. Kokubo, T., Bioactive Glass Ceramics: Properties and Applications. *Biomaterials* **1991,** *12*, 155-163.
39. Serajuddin, A. T. M.; Sheen, P.-C.; Augustine, M. A., Common Ion Effect on Solubility and Dissolution Rate of the Sodium Salt of an Organic Acid. *Journal of Pharmacy and Pharmacology* **1987,** *39* (8), 587-591.
40. Jäger, C.; Welzel, T.; Meyer-Zaika, W.; Epple, M., A Solid-State NMR Investigation of the Structure of Nanocrystalline Hydroxyapatite. *Magnetic Resonance in Chemistry* **2006,** *44* (6), 573-580.

41. MacKenzie, K. J. D.; Smith, M. E., *Multinuclear Solid-State NMR of Inorganic Materials*. 2002; Vol. 6, p 727.

42. Cheetham, A. K.; Clayden, N. J.; Dobson, C. M.; Jakeman, R. J. B., Correlations Between ^{31}P N.M.R. Chemical Shifts and Structural Parameters in Crystalline Inorganic Phosphates. *Journal of the Chemical Society, Chemical Communications* **1986,** (3), 195-197.

43. Chen, Q.; Thouas, G., *Biomaterials: A Basic Introduction*. CRC Press: Florida, USA, 2018; p 740.

44. Bohner, M.; Lemaitre, J., Can Bioactivity Be Tested in vitro with SBF Solution? *Biomaterials* **2009,** *30* (12), 2175-2179.

45. Olivieri, M. P.; Kittle, K. H.; Tweden, K. S.; Loomis, R. E., Comparative Biophysical Study of Adsorbed Calf Serum, Fetal Bovine Serum and Mussel Adhesive Protein Films. *Biomaterials* **1992,** *13* (4), 201-208.

46. Seredych, M.; Mikhalovska, L.; Mikhalovsky, S.; Gogotsi, Y., Adsorption of Bovine Serum Albumin on Carbon-Based Materials. *C* **2018,** *4* (1), 3.

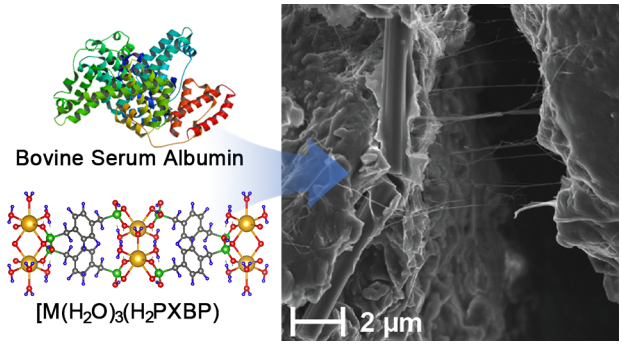
Bovine Serum Albumin
[M(H2O)3(H2PXBP)
2 µm